Lake level changes in the Tibetan Plateau from Cryosat-2, SARAL, ICESat, and Jason-2 altimeters

Cheinway Hwang[1, *], Yung-Sheng Cheng[1], Wan-Hsin Yang[1], Guoqing Zhang[2], Yong-Ruei Huang[1],
Wen-Bin Shen[3], and Yuanjin Pan[3]

[1] *Department of Civil Engineering, National Chiao Tung University, Hsinchu, Taiwan*
[2] *Institute of Tibetan Plateau Research, Chinese Academy of Sciences, Beijing, China*
[3] *School of Geodesy and Geomatics, Wuhan University, Wuhan, China*

ABSTRACT

Lake level change in the Tibetan Plateau is an important indicator for regional and global climate changes. We use altimeter data from Cryosat-2, SARAL, ICESat, and Jason-2 to detect lake level changes at different spatial and temporal resolutions over 2003 - 2017 (Jason-3 data in 2017 for validation). Cryosat-2's SARIn mode provides precise water level time series over 59 lakes. SARAL's waveforms are re-tracked to generate near monthly, high-quality measurements at 31 lakes. Jason-2 provides a reference for removing inter-altimeter biases, enabling coherent records over lakes with Jason-2 passes. After a decade of rise since the ICESat record of 2003, the lake levels of Nam Co, Selin Co, Ngangzi Co, and Chibuzhang Co became flat in 2014 - 2016 and started to fluctuate or decline after 2016. Such positive-flat-negative trends are consistent with the trend variations of mass change from Gravity Recovery and Climate Experiment (GRACE). SARAL detected persistent lake level declines over 2013 - 2016 in southern Tibet that may signify the onset of decadal reduced flows of the Yarlung Tsangpo and Brahmaputra River that could affect the water supply for their downstream regions in India and Bangladesh. Cryosat-2 and Jason-2 detected sudden lake level rises and falls around Zhuonai, Kusai, and Salt Lake associated with a 2011 lake outburst, which is confirmed by lake volume changes from two Landsat-7 images. With a careful processing and calibration, multiple altimeters allow for determining and cross-validating long-term and episodic lake level changes unachievable by a single altimeter.

1. INTRODUCTION

The Tibetan Plateau (TP) is covered with numerous large natural lakes, especially in the Inner TP. The space and time evolutions of lakes here are mostly the results of local and global hydrological changes, which are often interpreted as a manifestation of regional and global climate change (Kang et al. 2010; Hwang et al. 2011; Liao et al. 2013; Crétaux et al. 2016; Zhang et al. 2017a). However, due to the vastness and remoteness of the TP, most lakes here lack in situ measurements of water level, making it difficult to understand the long-term spatial and temporal characteristics of their evolution and dynamics.

This difficulty of sampling lake level changes in the TP can be reduced by using measurements from remote-sensing sensors. Several remote sensing techniques have shown how lakes in the TP evolve over space and time (Zhang et al. 2011, 2013, 2014, 2017a, b). One technique is based on optical imagery from satellites or aircrafts (recently, unmanned aerial vehicles), which is typically used to detect lake area changes (Zhang et al. 2014, 2017a). Sample studies using satellite imagery in the TP are Shao et al. (2008), Huang et al. (2012), and Yao et al. (2013). Another remote technique is satellite altimetry, which can measure lake levels and their changes. There are numerous studies documenting satellite altimeter results of lake level changes in Tibet. For example, Zhang et al. (2011) used Ice, Cloud, and the land Elevation Satellite (ICESat) data to determine Tibetan lake level changes from 2003 to 2009, concluding that the overall lake

levels were on the rise. Kleinherenbrink et al. (2015) used Cryosat-2 (C2) data to detect lake level changes in Tibet and Tianshan area, which were then assessed by the result from Jason-2 (J2). A recent study by Jiang et al. (2017) using C2 suggests that 68.6% of the lakes underwent rising lake level trends. In these studies, seasonal lake levels were not statistically significant because ICESat and C2 observe lake levels at time intervals exceeding one month or longer.

By contrast, seasonal lake level changes can be easily detected by repeat altimeter missions. For example, Zhang et al. (2015) used altimeter data from the 10-day repeat TOPEX/Poseidon (T/P) mission and 35-day repeat Envisat mission to determine lake level changes of Zhari Nam Co, showing that lake level oscillations in springs and winters were much larger than the oscillations in summers and falls. Hwang et al. (2016) used T/P-family satellites to observe seasonal and two decades of lake level changes at 23 lakes in Tibet. Crétaux et al. (2016) used satellite altimetry to calculate lake water storage changes in Tibet in order to study their inter-annual variability. Finally, Tseng et al. (2016) used data from ICESat, J2, and Envisat to detect the long-term variations of lake level over Dorsoidong and Chibuzhang Co, suggesting that the two lakes were merged due to the rising runoffs from the nearby glaciers near Mt. Tanggula.

These altimeter studies in the TP suggest that both long-period and short-period missions can be used for lake level changes, despite their shortcomings in either spatial or temporal resolution. Missions such as ICESat and C2 can greatly increase spatial coverages, but they were unable to detect seasonal changes over small lakes. Missions such as T/P and Envisat can provide lake level observations at 10- and 35-day intervals, but their spatial coverages are low because of the large cross-track intervals of 315 and 75 km of the two missions. In general, the order of decreasing spatial resolution is: C2 > ICESat > Envisat or SARAL/AltiKa (SA) > T/P satellites, while the order of decreasing temporal resolution is T/P satellites > Envisat or SA > C2 > ICESat. Therefore, the best strategy is combing altimeters of different mission characteristics to increase both the spatial and temporal resolutions. According to Crétaux et al. (2009), Fu and Haines (2013), and Hwang et al. (2016), we need to remove inter-altimeter biases to obtain coherent, continuous lake level observations when using multiple satellites. Such biases may be identified using in situ height measurements, but only few lakes in the TP are equipped with lake gauges (Zhang et al. 2017a, b).

In addition to long-term lake level records from multiple altimeters, another issue is the reliability and interpretation of altimeter-detected episodic lake level changes caused by extreme events such as flooding and glacier avalanche. For example, J2 detected a sudden, large lake level rise over Kusai Lake caused by an extreme precipitation event (Hwang et al. 2016), but J2 alone cannot show how Kusai Lake received the water from its upstream lakes, nor

its' lake level measurements can reveal volume changes of lakes around here.

With the background analysis, this study focuses on the value of multiple altimeters in detecting both the long-term (> the time span of one mission) and short-term (few months) lake level changes in the TP. The first objective is to determine lake level changes from C2, SA, J2, and IC-ESat, and examine how such results reveal long-term lake level trends and how such trends are compared with the mass change trends from GRACE (Tapley et al. 2004). The second objective is to show how multiple altimeters and Landsat-7 imagery can identify source waters contributing to the 2011 lake outburst event in northern Tibet (Hwang et al. 2016).

2. DATA AND METHODS

2.1 Altimeter Data

C2 was launched by the European Space Agency (ESA) on 8 April 2010 and has a repeat period of 369 days in its main cycles and a 30-day repeat period in its sub-cycles. C2 carries a Ku-band SAR/Interferometric Radar Altimeter to measure ranges between the satellite and the earth's surface in three different modes, i.e., the Low Resolution Mode (LRM), Synthetic Aperture Radar (SAR), and SAR/Interferometric Radar Altimeter (SARIn) mode (Bouzinac 2013). Over the most TP, C2 uses the SARIn mode to measure surface heights, resulting in a much higher resolution than that in the LRM mode. The C2 data used in this study were downloaded from the site at ftp://science-pds.cryosat.esa.int, spanning from April 2010 to June 2016.

SA is a joint mission of the Indian Space Research Organization (ISRO) and the France space agency (CNES). The mission, launched on 25 February 2013, is a continuation of the ERS series and Envisat missions. Since October 2013, SA followed exactly the ground tracks of Envisat in a 35-day repeat orbit, and carries a Ka-band altimeter, called AltiKa. The original range sampling rate of SA is 40 Hz. A SA waveform contains 128 gates with the default tracking gate at 55. In July 2015, SA experienced an attitude control problem, resulting in ground tracks that are up to 8 km off SA's nominal repeat ground tracks (https://www.aviso.altimetry.fr/en/missions/current-missions/saral.html). Because of such offsets, after July 2015 SA failed to collect lake level observations over some small lakes. We downloaded the needed SA data from ftp://avisoftp.cnes.fr, spanning from March 2013 to May 2016.

ICESat was launched by the National Aeronautics and Space Administration (NASA) on 13 January 2003. ICESat was part of NASA's Earth Observing System and carried the Geoscience Laser Altimeter System (GLAS) to measure surface elevations at a 40-Hz rate. The ICESat mission ended in 2009, and it has a good performance on lake level studies of Tibet (Zhang et al. 2011). We obtained the version 34 of ICESat data from the web site: https://nsidc.org/data/

GLAH14/versions/34 over January 2003 to October 2009.

The J2 mission, launched on 20 June 2008, is a continuation of the T/P and Jason-1 missions. J2 is a joint mission of NASA, CNES, the European Organization for the Exploitation of Meteorological Satellites (EUMETSAT) and the National Oceanic and Atmospheric Administration (NOAA). With its 10-day repeat period, J2 provides lake measurements with the highest temporal resolution among all past and ongoing altimeters, but its large cross-track spacing results in the least number of observed lakes. The J2 data were downloaded from ftp://avisoftp.cnes.fr. The time period of the J2 altimeter data used spanned from June 2008 to December 2016.

2.2 Selecting and Screening Altimeter Data

For all altimeters, our data processing procedure is similar to the one used in Hwang et al. (2016), and is presented in three steps for the four altimeters as follows.

Step 1: Selecting altimeter data over a lake water surface

First, the Google Earth was used to determine the lake's coverage. Any altimeter data within 2 km to the lake's shores were ignored. Although Landsat imagery can provide a higher spatial resolution of lake boundaries, this technique was not used in the paper due to limited resources. For example, Fig. 1 shows a C2 track over Nam Co and altimeter waveforms along this track (the waveforms are not on consecutive points). For example, Fig. 1 shows a C2 track over Nam Co and altimeter waveforms along this track. The waveforms on land (point No. 1 - 3 and 8) are corrupted and significantly different from those over Nam Co (point No. 4 - 7), which are considered usable for gener-

ating lake height observations. Under this selection criterion (an altimeter observation cannot be within 2 km to a lake's shore), many small lakes (area < 27 km^2) was disregarded.

Step 2: Applying corrections to raw measurements

An altimeter measures lake levels using the radar or laser ranges between the satellite and a lake's surface. Lake level measurements can be computed as (Hwang et al. 2016):

$$H_{lake} = h_{sat} - R_{alt} - C \tag{1}$$

$$C = C_{COG} + C_{wet} + C_{dry} + C_{iono} + C_{solid} + C_{pole} + C_{retrack} \tag{2}$$

Where H_{lake}: ellipsoidal height of lake; h_{sat}: ellipsoidal height of satellite; R_{alt}: range between altimeter and lake surface; C: sum of all corrections, including center of mass correction (C_{COG}), wet and dry tropospheric corrections ($C_{wet} + C_{dry}$), ionospheric correction (C_{iono}), solid earth tide (C_{solid}), pole tide (C_{pole}), and retracker correction ($C_{retrack}$). Except C_{solid} and C_{pole}, these corrections are satellite-dependent. Over lakes in Tibet, there is no need to apply corrections for ocean tide correction, inverse barometer correction, and sea state bias correction (Hwang et al. 2016). All corrections in Eq. (2) are provided in the altimeter datasets presented in section 2.1, except the retracker corrections for SA and J2. Currently, the data center of ICESat does not provide its waveforms for retracking, nor retracker corrections. We determined the retracker corrections for SA and J2 using the subwaveform retracking method of Yang et al. (2012). A detailed numerical procedure for this computation is already presented in Hwang et al. (2016) and will not be repeated here.
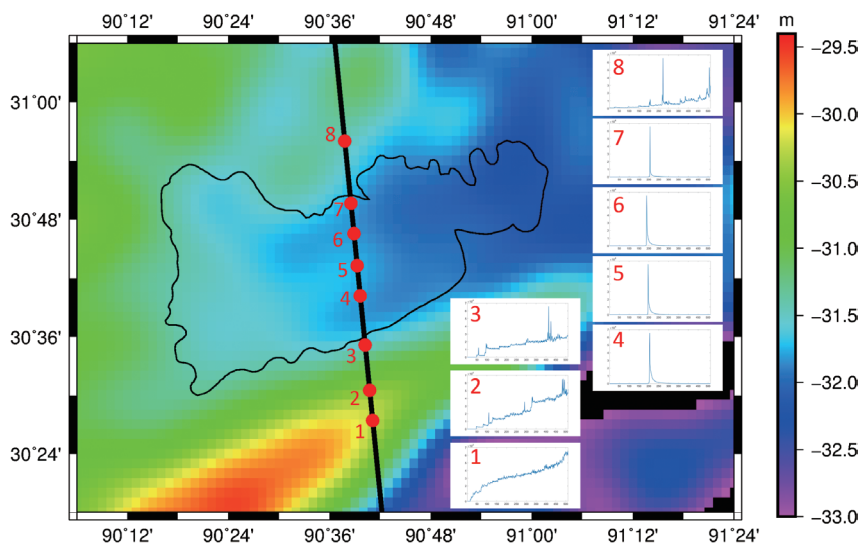

Fig. 1. A Cryosat-2 track over Nam Co with geoidal heights from EGM08. Geoidal differences on the western and eastern sides of Nam Co exceeds 1 m. Inserted are altimeter waveforms at 8 locations over land and Nam Co's surface. The waveforms at point No.4 - 7 are specular and are considered usable waveforms.

For C2, we used directly lake level observations from SGDR-L2 product, including the wet and dry tropospheric corrections, ionospheric correction, solid earth tide, pole tide, and retracker correction. The retracker corrections of Wingham/Wallis for the SARin-mode observations in the SGDR-L2 product of C2 can be found at https://earth.esa.int/documents/10174/1773005/C2-Evolution-BaselineC-Level2-V3.

Step 3: Outlier removal

After the data selection and the retracking correction in the previous two steps, there are still outliers in lake level observations. Such outliers can cause errors when forming mean lake levels and computing rates of lake level change (section 2.3). As such, we employed an additional step to remove outliers. Outliers are iteratively removed until all anomalies (individual observations relative to the mean of observations) fall within 2.5 standard deviations (Hwang et al. 2016).

2.3 Correction for Geoid Gradient and Determinations of Lake Level Time Series and Trends

Over a given lake, for each altimeter cycle or sub-cycle we formed a mean height (see $\bar{h}$ below) from the outlier-free height measurements along the ground track(s) passing the lake (see step 3 in section 2.2). Before forming the mean height, the along-track heights were reduced to heights at a reference point, which is roughly at the center of the lake [see (φ_0, λ_0) below, and the latitudes and longitudes in Appendix A]. This reduction is called the geoid gradient correction. The difference between the geoidal heights at the reference point and the measurement location was computed and then added to the altimeter-determined lake level. The geoidal heights were determined from the EGM08 geoid model (Pavlis et al. 2012). The geoidal variation over a large lake can be significant. For example, Fig. 1 shows that the differences between the geoidal heights on the west coast and the east coast of Nam Co are more than 1 m (Jiang et al. 2017). Over a lake the size of Nam Co, the lake surface is not a surface of constant orthometric height. Neglecting geoidal differences can introduce large errors when computing the mean height from the along-track heights.

These mean lake heights are treated as "pseudo" observations over a lake and are fitted by the function:

$$\bar{h}(\varphi_0, \lambda_0, t) + v = a + b(t - t_0) + c\cos\omega(t - t_0)$$
$$+ d\sin\omega(t - t_0) \qquad (3)$$
$$\text{weight} = p$$

where $\bar{h}(\varphi_0, \lambda_0, t)$ is the mean height (after the geoid gradient reduction) at the center of the lake (φ_0, λ_0), t is the time for $\bar{h}$, and t_0 is the central time of a satellite mission's time span, v is residual, a is the mean lake level over the time span, b is the rate of lake level change, c and d are terms for annual variation, ω is the annual frequency (one cycle per year), and p is the weight for $\bar{h}(\varphi_0, \lambda_0, t)$. In this study, p is the number of heights that are used to form $\bar{h}(\varphi_0, \lambda_0, t)$. It turns out the number of lake level measurements can vary from one repeat cycle to another over the same lake. In addition, p is larger over a larger lake like Nam Co, where an altimeter mission may have more than one ground track and the ground track(s) can be relatively long; over a small lake, p can be small because the lake may have just one short altimeter ground track.

2.4 Constructing Inter-Satellite Lake Level Records

This study uses four altimetry satellites to study lake level changes. These satellites use different altimeters and reference ellipsoids. Their differences are summarized as follows [see also Eqs. (1) - (2)]. (1) ICESat uses laser, while the other satellites uses pulse-limited radar. (2) J2 and C2 (conventional radar) use the Ku-band radar. (3) SA uses a Ka-band radar. (4) C2 uses the SARIn mode in the TP. (5) Ionospheric delays over lakes can be from the dual or tri-band altimeter measurements or from a numerical model. (6) The reference frames for different satellite missions can be different. Fu and Haines (2013) have presented a review on these differences for long-term sea level monitoring, but not for lake level monitoring.

Because of these differences between the four missions, range biases could exist between lake levels over the same spot of a lake from these four different altimeters (Crétaux et al. 2009, 2016; Fu and Haines 2013; Hwang et al. 2016). For example, Fig. 2a shows the lake level time series from three altimeters over Selin Co. Here the ICESat time series has a clear shift with respect to those from C2 and SA. Therefore, it will be a challenge to connect the lake measurements from ICESat, C2 and SA to form a long-term record of Selin Co's lake level changes.

One method for removing inter-altimeter biases is one that based on in situ lake gauge measurements. For example, Song et al. (2015) removed a bias between the ICESat and C2-derived lake levels over Nam Co using in situ lake level observations. In Fig. 2b, we repeat the approach of Song et al. (2015) to remove the bias between ICESat and C2 over Nam Co, where we obtained the lake gauge measurements from Zhang et al. (2011) and Song et al. (2015). The standard deviation between the C2 and in situ observations over the overlapping period is 0.25 m and the correlation is about 0.94. However, only few lakes in Tibet have in situ observations, so this method of altimeter bias removal can only be used in limited cases.

Another method of bias removal is based on comparison with the J2 result. J2 delivers highly accurate lake level measurements in Tibet, such measurements can be used to calibrate those from other satellites. However, J2 can serve
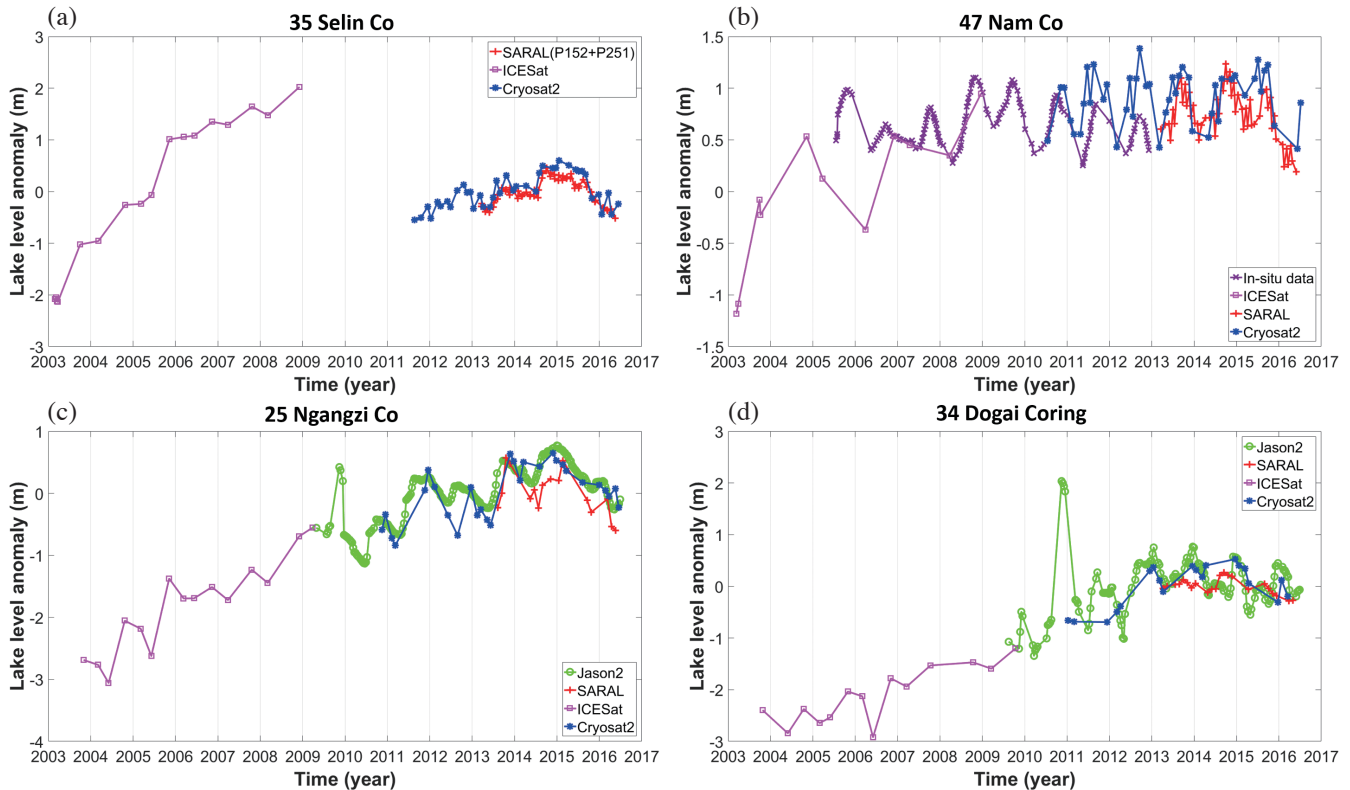
Fig. 2. (a) Lake level changes in Selin Co from three satellites, showing a large inter-satellite bias between ICESat and the other altimeters. (b) Lake level changes in Nam Co from three satellites and lake-gauge data, adjusted by in situ level measurements. Lake levels over (c) Ngangzi Co, (d) Dogai Coring, which are adjusted to the lake level measurements of Jason-2.

this function only over a lake when the lake contains at least one J2 track. Here we show an example of C2 and ICESat lake level calibrations using J2 data over Ngangzi Co (Fig. 2c). First, we determined the mean difference between ICESat and J2 lake level heights (absolute height at the same location), which is 1.72 m. We repeated this process to obtain a mean height difference of 0.27 m between C2 and J2 over Dogai Coring (Fig. 2d). Both the results in Figs. 2c and d suggest that J2 can help to eliminate the lake level differences between ICESat and C2. Again, this bias removal is valid only if a lake is visited by J2.

3. RESULT

3.1 Rates of Lake Level Change

We constructed time series of lake level change from the four satellites. As comprehensive results of ICESat and J2 studies of lake level changes in the TP have been presented in, e.g., Zhang et al. (2011) and Hwang et al. (2016), we only focus on the results from the ongoing C2 and SA altimeters. The C2 altimeter data result in time series of lake level change at 59 lakes, while SA results in 31 series. Note that we use a different altimeter data screening criterion (section 2.2) than that used in Jiang et al. (2017), leading to different numbers of selected lakes between the two studies. Appendix A provides the geodetic coordinates, areas, mean elevations of the selected lakes for the C2 and SA altimeters, and lake names in Chinese, English and Tibetan. The IDs for lakes in Appendix A are for convenient references in the results presented below. Of the 31 lakes with rates from SA in Appendix A, 29 lakes have rates also from C2. Table 1 shows the lake level trends derived from C2 and SA. Because an outburst event occurred over Kusai Lake in 2011 (ID 55, section 3.2), Table 1 also shows the lake's rates of water level changes over 2010 - 2012, 2012 - 2016, and 2010 - 2016. In general, the standard errors of the estimated rates in Table 1 are below 0.10 m year^{-1}. A sample discussion on the uncertainties of altimeter-derived rates of lake level change was presented in Gao et al. (2013); this subject will not be discussed further in this paper.

Figure 3a shows the C2-derived lake level trends over 2010 - 2016. In total, 37 lake levels were on the rise, while the lake levels at 22 lakes declined. Figure 3b shows the lake level trends at the 31 lakes from SA over 2013 - 2016. Of the 31 lakes from SA, 14 were rising, while 17 were falling. Table 1 shows that over some lakes the rates from SA and C2 have opposite sign. This is partially due to the different time spans of C2 and SA, and the fact that SA has a 35-day repeat period that is shorter than that of C2. In addition, the following two factors may contribute to the

Table 1. Lake level change rates from Cryosat-2 (2010 - 2016) and SARAL/AltiKa (2013 - 2016) (unit: m year^{-1}).

| ID[1]	Name	Cryosat2 (2010 - 2016)	SARAL (2013 - 2016)	ID[1]	Name	Cryosat2 (2010 - 2016)	SARAL (2013 - 2016)
1	Aksayqin Lake	0.20 ± 0.04	-	33	Linggo co	0.65 ± 0.08	-
2	Songmuxi Co	0.00 ± 0.07	-	34	Dogai Coring	0.15 ± 0.05	-0.07 ± 0.03
3	Jieze Caka	0.20 ± 0.05	0.07 ± 0.03	35	Selin Co	0.10 ± 0.03	0.04 ± 0.03
4	Gozha Co	-0.25 ± 0.12	-	36	Dogaicoring Qangco	-0.01 ± 0.04	0.01 ± 0.03
5	La'nga Co	-0.16 ± 0.06	-0.22 ± 0.03	37	Jingyu Lake	0.07 ± 0.03	0.13 ± 0.06
6	Mapam Yumco	0.00 ± 0.04	-0.09 ± 0.05	38	Dorsoidong Co	0.40 ± 0.06	0.21 ± 0.05
7	Bamgdog Co	0.62 ± 0.02	0.52 ± 0.03	39	Botao Lake	-0.04 ± 0.07	-
8	Lumachangdong Co	0.33 ± 0.03	0.23 ± 0.03	40	Kyebxang Co	0.00 ± 0.02	-
9	Pur Co	-0.05 ± 0.06	-	41	Laorite Co	-0.1 ± 0.07	-
10	Heishi North Lake	0.40 ± 0.05	0.26 ± 0.03	42	Lexie Wudan Lake	0.36 ± 0.03	0.22 ± .015
11	Ngangla Ringco	-0.06 ± 0.02	-0.17 ± 0.03	43	Chibuzhang Co	0.42 ± 0.06	0.20 ± 0.05
12	Bairab Co	-0.02 ± 0.02	-	44	Xijir Ulan Lake	-0.13 ± 0.03	-
13	Salt Water Lake	0.15 ± 0.07	-	45	Wulanwula Lake	-0.01 ± 0.03	-0.04 ± 0.03
14	Rinqin Xubco	0.08 ± 0.07	-	46	Puma Yumco	-0.17 ± 0.07	-0.09 ± 0.04
15	Taro Co	-0.09 ± 0.02	-0.31 ± 0.05	47	Nam Co	0.03 ± 0.03	-0.09 ± 0.03
16	Lagkor Co	0.14 ± 0.11	-	48	Mingjing lake	0.39 ± 0.07	-0.15 ± 0.15
17	Yamzhog Yumco	0.36 ± 0.11	-	49	Taiyang Lake	0.07 ± 0.09	-
18	Dong Co	0.00 ± 0.03	-0.04 ± 0.02	50	Zige Tangco	0.1 ± 0.04	-
19	Dagze Co	0.07 ± 0.03	-	51	Hoh Xil Lake	0.26 ± 0.05	-
20	Peiku Co	0.03 ± 0.04	-	52	Zhuonai Lake	-2.06 ± 0.52	-
21	Zhari Nam Co	0.01 ± 0.01	-0.11 ± 0.03	53	Cuorendejia	-0.13 ± 0.09	-0.03 ± 0.08
22	Yi'bug Caka	-0.14 ± 0.15	-	54	Telashi Lake	0.25 ± 0.05	-
23	Yurbao Co	0.63 ± 0.11	-	55	Kusai Lake	0.4 ± 0.38	-0.07 ± 0.02
24	Margai Caka	0.24 ± 0.05	-		Kusai Lake (2010 - 2012)	7.91 ± 2.77	-
25	Ngangzi Co	0.12 ± 0.04	-0.20 ± 0.08		Kusai Lake (2012 - 2016)	-0.21 ± 0.05	-
26	Dagze Co	0.08 ± 0.03	0.10 ± 0.04	56	Salt Lake	0.78 ± 0.06	-
27	Urru Co	-0.07 ± 0.05	-	57	Gyaring Lake	0.02 ± 0.04	-0.04 ± 0.03
28	Xianhe Lake	0.19 ± 0.05	-	58	Eling lake	-0.19 ± 0.08	-0.19 ± 0.05
29	Yinbo Lake	0.38 ± 0.05	-	59	Donggei Cuona Lake	0.08 ± 0.03	-
30	Pongyin Co	0.03 ± 0.05	-	60	Alake lake	-	0.14 ± 0.03
31	Xuemei lake	0.42 ± 0.07	0.15 ± 0.03	61	Qinghai Lake	-	0.03 ± 0.02
32	Gyaring Co	-0.22 ± 0.08	-0.34 ± 0.08				
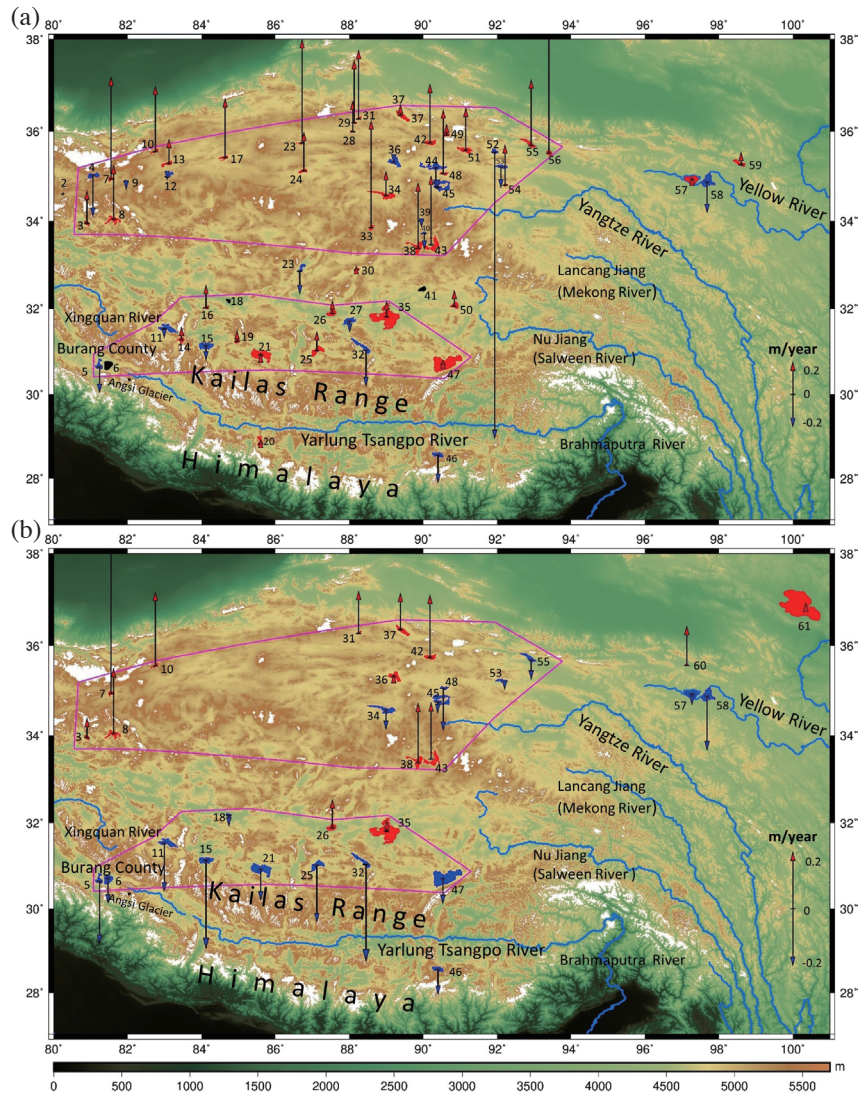
Fig. 3. Rates of lake level change from (a) Cryosat-2 at 61 lakes (2010 - 2016), (b) SARAL/AltiKa at 31 lakes (2013 - 2016). The geodetic coordinates and IDs of the lakes are shown in Appendix A. The two polygons show the boundaries for computing the trends of GRACE-derived mass changes in Fig. 5. The polygon in southern Tibet is so chosen that the Himalayas are not included.

different signs: (1) SA repeats its ground track within 1 km and tends to be less affected by modeled geoidal differences from EGM08 and (2) SA's data volumes are stable from one cycle to another, compared to C2's data volumes. More studies are needed to clarify the differences between C2 and SA over the same lakes in Table 1. Despite these differences, Figs. 3a and b show that, in general, the lake levels in western and northern Tibet were rising, while those in southern Tibet were falling.

3.2 Comparisons Between Lake Level Changes from Cryosat-2 and SARAL

In addition to Fig. 2, Fig. 4 shows the time series of lake level change from C2 and SA at selected lakes in connection to the C2 and SA results in Table 1. Figure 4 also includes

Jason-3 and extended C2 records, which will be discussed in section 4.1.1. In Fig. 4, the SA-derived rates confirm the rates from C2, thus showing the value of a repeat mission like SA (or its sister missions like the Sentinel series, see https://earth.esa.int/web/sentinel/missions) in validating results from an altimeter mission with the characteristics of C2, or from ICESat-2 (https://icesat-2.gsfc.nasa.gov). Furthermore, in most cases the seasonal variations from C2 are consistent with those from SA (Fig. 2).

A large number of studies have analyzed the causes of the past and recent lake level changes in Tibet. For example, Jiang et al. (2017) found that lake level changes in Tibet were strongly related to temperature changes. Zhang et al. (2017a) attributed recent lake expansions to increased precipitations and meltwater from glaciers. In general, temperature rising rates in Tibet were 2 times more than the global average rate

(Kang et al. 2010; Liao et al. 2013). In this study, our aim is not to repeat such lake level-climate factor analyses, which are largely based on lake level measurements up to 2014 or 2015. Instead, in section 4, we will discuss two subjects: (1) decadal lake level trends and onsets of declines over selected lakes and connections to the GRACE result, and (2) a 2011 lake outburst detected by the J2 and C2 altimetry.

4. DISCUSSION

4.1 The Post-2016 Trend of Lake Level

4.1.1 The Decadal Change Signal: Extending Lake Level Records

We notice that, the lake levels of Selin Co (Fig. 2a), Nam Co (Fig. 2b), Ngangzi Co (Fig. 2c), and Dogai Coring (Fig. 2d) started to decline since around 2014 - 2016 after more than a decade of lake level rise (but note the result when the Jason-3 data are added). In two previous studies (Hwang et al. 2005, 2016), it was found that the lake levels of Ngangzi Co (ID 25) have opposite trends before and after the 1997 - 1998 El Niño. The 2015 - 2016 El Niño is the largest El Niño since the 1997 - 1998 event (Levine and McPhaden 2016). Zhai et al. (2016) showed that it has affected the climate in China. Specifically, this event increased the temperatures and droughts in northern China. But whether this 2015 - 2016 event has any connections to climate change in the TP has not been reported.

The flat rates in Fig. 2 around 2014 - 2016 seem to indicate a possible onset of a new trend of lake level change in the TP, which might affect the long-term (at decadal levels or longer) supplies of source water to the major rivers originating from Tibet (Fig. 3), such as the Yangtze River, the Yellow River, and the Yarlung Tsangpo River (see more discussions using extended lake records and GRACE results below). Decadal climate variability has become increasingly important for predicting the long-term climate effect on water resource, agriculture and natural hazards (Navarra 1999; Liu 2012). As shown by Liu (2012), decadal changes can be of stochastic and deterministic nature: a stochastic decadal change can be triggered by an event such as El Niño or La Niña and has no clear onset time. A deterministic decadal change can be related to periodic phenomena such as the 11-year solar cycle (Liu 2012). As it happened, the years 2014 - 2016 belong to the warm phase of the El Niño Southern Oscillation (ENSO). But it is beyond the scope of this paper to investigate whether this 2015 - 2016 El Niño has initiated the lake level decline around 2014 - 2016 seen in Fig. 2. Incidentally, recent papers dealing with Tibetan lake levels, e.g., Hwang et al. (2016) and Jiang et al. (2017), show altimeter records in Tibet only up to about 2014 and early 2015. According to the predictions of Yang et al. (2018), precipitation and lake area in the inner Tibetan Plateau will continue to increase over 2016 - 2025, but with lower rates compared

to the pre-2016 rates. The post-2016 altimeter data in Tibet can provide examinations for such predictions.

Here we provide a preliminary examination of the post-2016 lake level trends by extending the lake level records of three lakes in Fig. 2 and that of Chibuzhang Co to the latest possible date (note: the rates in Fig. 3 are based on altimeter data up to early 2016). Whenever possible, we also include lake level records from Jason-3 (the follow-on mission of Jason-2, launched in January 2017). Figure 4 shows the extended lake levels over lakes that have signs of the lake level decline (three lakes in Figs. 2a - c, plus Chibuzhang Co in Fig. 4d). Note that, due to a time constraint, the extension is relative to the results in Figs. 2 and 3 only; we cannot obtain altimeter data to extend the record over Dogai Coring in Fig. 2d. In Fig. 4a, we manually lowered ICESat's measurements to make a smooth transition for all the measured lake levels in Fig. 4a. The result shows that Selin Co's lake level has been rising since the beginning of ICESat's records (2003), reaching a peak in early 2015 and starting to decline after 2016. The extended C2 records show a continuous decline of Nam Co lake level after 2016.

The extended records from Jason-3 over Ngangzi (Fig. 4c) and Chibuzhang Co (Fig. 4d) show mixing results. Over these two lakes, the rates from J2, SA and C2 turn from positive values to negative values around 2014 - 2016. While Jason-3 shows fluctuating lake levels of Ngangzi Co after 2016, surprisingly it indicates that the lake level of Chibuzhang Co continues to rise after 2016. Since Chibuzhang Co receives meltwater from Mt. Tanggula, where the glaciers are rapidly retreating (Chao et al. 2017), the post-2016 lake level rise of Chibuzhang Co from Jason-3 may indicate accelerated meltwater from Mt. Tanggula.

4.1.2 Lake Level Change and Mass Change

The post-2016 lake level trend can be compared with that of an independent parameter such as mass change. In this paper, we use mass changes derived from the GRACE gravity mission (Tapley et al. 2004) to examine a potential link between the lake level trends seen in Figs. 2 and 4 and the mass trends from GRACE. Figure 5 shows the time series of monthly mass change within the polygons (Figs. 3a and b) in northern (Fig. 5a) and southern Tibet (Fig. 5b). The two time series in Fig. 5 were conveniently obtained from the GRACE Plotter at http://www.thegraceplotter.com, where we chose the solution CSR RL05 DDK5 for the result in Fig. 5 (note: GRACE solutions on the GRACE Plotter are available up to early 2016). This solution is from the Release 5 of the GRACE Level 2 data, the Center for Space Research, at the University of Texas. The DDK5 filter was described in Kusche et al. (2009). In addition, we did not remove the effect of glacier isostatic adjustment from the GRACE-derived gravity changes, which is small in Tibet and will not exhibit any decadal trend (our targeted

signal). In Figs. 5a and b, we also show the smoothed EWH changes by applying the Gaussian filter to the original EWH values (the filtering window size is one year).

Figure 5a shows that, in northern Tibet the trends of mass change (in equivalent water height, EWH) from GRACE were consistently positive from 2003 to 2014, with a mean rate of about 1 cm/year in EWH (note: a value in the time series is the areal mean within the polygon defined in Fig. 3a; the same holds for the values in Fig. 5b). The mass increase

trend became flat some time near 2014 - 2016. The variation in the mass change rate in Fig. 5a appears to be similar to the variations in the lake level change rate in Figs. 2 and 4. Note that, the rates of lake level change in Fig. 3a from C2 are over 2010 - 2016, thus the signs of rates are mostly positive and are dominated by the positive changes before 2014. Because of C2's long repeat period and the resulting large uncertainties in the estimated rates, we did not show the rates of lake level change over 2013 - 2016 from C2.

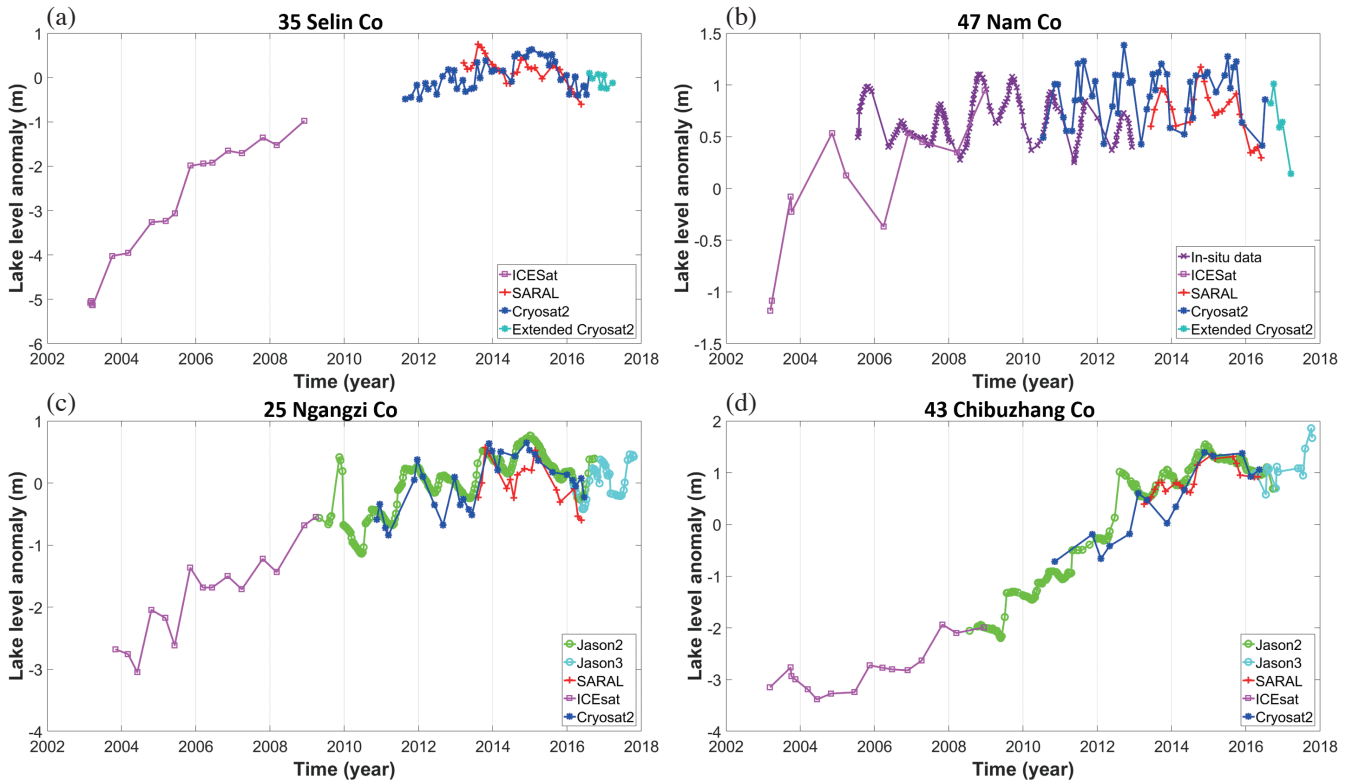Fig. 4. Extension of lake level records from early 2016 to March 2017 from C2, J2, and Jason-3 over (a) Selin Co, (b) Nam Co, (c) Ngangzi Co, and (d) Chibuzhang Co. For coherent lake level trends, shifts are applied to the ICESat records whenever needed.
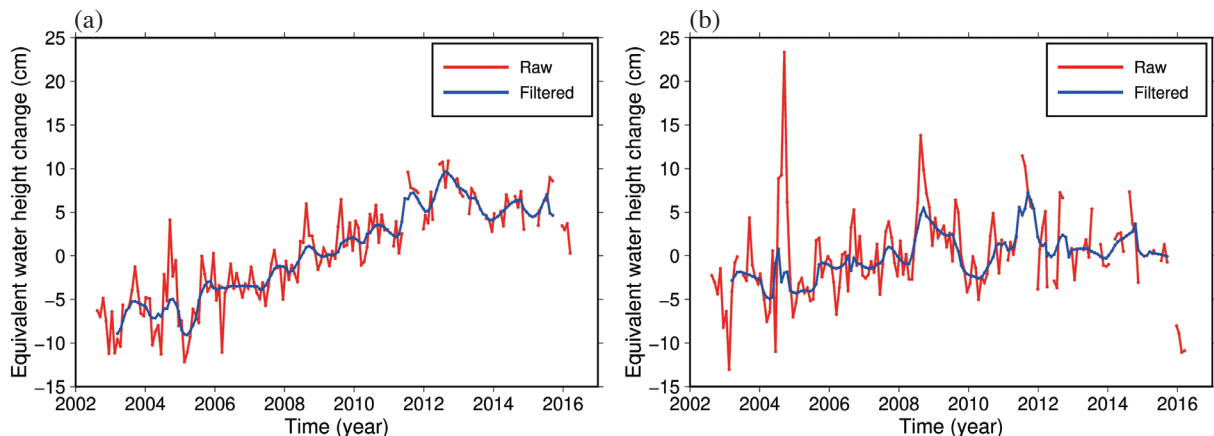

Fig. 5. Trends of GRACE-derived mass change in (a) northern Tibet (within the polygon in Fig. 3a) and (b) southern Tibet (within the polygon in Fig. 3b).

In southern Tibet, the trends of mass change and lake level change (Figs. 3b and 5b) were different from those in northern Tibet (Figs. 3a and 5a). The SA-derived lake level changes over 2013 - 2016 show negative signs (Fig. 3b; also the post-2014 lake level changes in Fig. 2), which are the results of lake level declines starting some time in 2014 - 2016 (an exact epoch for the start of the declines is not clear in Fig. 2). Like northern Tibet, southern Tibet has trends of mass change (Fig. 5b) that were persistently positive, but here the mean magnitude of mass change rate is 0.5 cm year^{-1}, about half that of northern Tibet. Again, like northern Tibet the rates of mass change in southern Tibet became flat some time in 2014 and then turned to negative values during 2014 - 2016. Note that the two time series of GRACE EWH in Fig. 5 contain large gaps after 2011, which were caused by the 40 - 50 days of GRACE's instrument shutdowns since April 2011 (Tapley et al. 2015). Despite these gaps, the declines of EWH values are evident in the two time series in Fig. 5. Furthermore, the EWH time series in Fig. 5b appears to be noisier than that in Fig. 5a, which is partially attributed to a smaller area used to define the southern Tibet (see the smaller polygon in Fig. 3).

In summary, the altimeter and GRACE results show that the trends of lake level change and mass change in the entire TP were positive from 2002 to around 2014, became flat (near zero) in 2014 - 2016, and lake levels at some lakes started to decline after 2016. But it remains questionable whether such declines will sustain into the next decade or longer, which can be answered by using long altimeter and GRACE (or its follow-on) records.

4.1.3 Lake Level Decline in Southern Tibet and the River Flows of Yarlung Tsangpo and Brahmaputra

The discussions in sections 4.1.1 and 4.1.2 raise an important issue: can the post-2016 declines in lake level and mass change in southern Tibet have any links to the flows of the rivers originating from Tibet? (See the major rivers in Fig. 3.) Immerzeel et al. (2010) showed that, while glacier meltwater plays a modest role for the flows of Yangtze River and Yellow River, it is extremely important for the Brahmaputra River. The Brahmaputra River is a major source of water for northeastern India and Bangladesh, and its upstream is the Yarlung Tsangpo River in southern Tibet (Fig. 3). The Yarlung Tsangpo River receives glacier meltwater from the Kailas Range to its north and from the Himalayas to its south. The lakes in southern Tibet (Fig. 3b) are mostly endorheic (Zhang et al. 2017b) and receive water from the Kailas Range and other sources. The Kailas Range is located between 78 and 90°E), and is at the northern side of the valley containing the entire Yarlung Tsangpo River (Fig. 3; see also search results by Baidu and http://www.igsnrr.ac.cn/kxcb/dlyzykpyd/zgdl/zgdm/200704/

t20070424_2154874.html). Since glaciers over the Kailas Range contribute meltwater to both the Yarlung Tsangpo River and the lakes in southern Tibet (Fig. 3), the onset of the decadal lake level decline and mass decline discussed in sections 4.1.1 and 4.1.2 may imply the beginning of a long-term (at least one decade) reduced flows of the Yarlung Tsangpo River and the Brahmaputra River due to less meltwater from the Kailas Range.

Because of the potential reduction of river flow in the Yarlung Tsangpo River, here we discuss the lake levels of La'nga Co and Mapam Yumco (IDs 5 and 6, Fig. 3). One of the glaciers that feed the two lakes is the Angsi Glacier, which is the origin of the Yarlung Tsangpo River (https://en.wikipedia.org/wiki/Angsi_Glacier). La'nga Co also receives inflows from the Xingquan River west of La'nga, which receives meltwater from glaciers in the Himalayas and the western Kailas Range. The Angsi Glacier is located at Burang County in southern Tibet, with latitude 30.2959°N and longitude 81.1772°E. In addition, subsurface caves and channels may exist between the two lakes, allowing Mapam Yumco to supply water to La'nga Co, which is at a lower altitude. The lake level of La'nga Co has been declining monotonically since the start of the T/P record in October 1992 (Hwang et al. 2016). The lake level of Mapam Yumco is governed by the glacier melt in the catchment area in its south (Biskop et al. 2016). Figures 6a and b show the time series of lake level change over La'nga Co and Mapam Yumco from C2, J2, and SA. The current rates of lake level change of Mapam Yumco are -0.09 m year^{-1} from SA and -0.01 m year^{-1} from C2 (no J2 result in Mapam Yumco). This implies that the lake level of Mapam Yumco is relatively steady compared to that of La'nga Co, which is -0.22 m year^{-1} from SA and -0.16 cm year^{-1} from C2. These results show that the lake level of La'nga Co is declining much faster than that of Mapam Yumco. In summary, the declining lake levels of the two lakes, together with the negative lake level rates in southern Tibet from SA (Fig. 3b), may signify decreasing glacier meltwater in southern Tibet and a potential decreased runoff of the Yarlung Tsangpo River that in turn reduces the flow of the Brahmaputra River.

4.2 The 2011 Lake Outburst Around Kusai Lake: Validation by Satellite Imagery

Here we discuss the large positive rate over Kusai Lake (No. 55) in Fig. 3. This rate is associated with a sudden lake level rise that has been detected by the J2 altimeter (Hwang et al. 2016). However, no remote sensing data were used to explain the sudden rise. According to Liu et al. (2016), two strong rainfall events near 22 August 2011 may have led to the lake level rise over Kusai. After these two events, persistent rainfalls continued in 2011 to raise the lake level of Zhuonai Lake, which is located in the upstream of Kusai. The strong rains and two major earthquakes combined to

induce the outburst of Zhuonai Lake, which caused the large lake level rises at Kusai and Salt Lakes.

Here we use the altimeter data from C2 and J2 as well as satellite imagery to investigate this 2011 lake outburst event. First, Fig. 7 shows the locations of the lakes around Kusai. Zhuonai Lake is in the upstream of Kusai, providing source water to the latter. East of Kusai lie two major lakes, Haidingnuover Lake and Salt Lake. Figure 8 shows two Landsat-7 images around Kusai Lake and Salt Lake on 23 November 2010 (before the outburst) and 12 November 2012 (after the outburst). These two images were obtained from United States Geological Survey (USGS) public site (https://earthexplorer.usgs.gov). To avoid the seasonal variation over the lake, we chose two images in the same season to minimize errors in estimating lake volume changes. It is clear that the two images show different lake coverages due to the flooding related to the lake outburst.

The J2 satellite travels through only Kusai Lake, rather than Zhuonai and Salt Lakes, making J2 unable to detect the consequence of Zhuonai's lake outburst (i.e., the sudden rise of Kusai lake level). That is, J2 alone cannot see both the cause and consequence of the outburst of Zhuonai. On the other hand, because C2 passes over the three lakes, C2's lake level observations can explain the origin and the result of the lake outburst. Figure 9 shows the C2-derived lake level changes over Zhuonai, Kusai and Salt Lakes, indicat-

ing dramatic lake level drops of Zhuonai Lake (Fig. 9a) and sudden level rises over Kusai and Salt Lakes (Figs. 9b and c) in 2011, which are consistent with the result of Liu et al. (2016). We find that (by C2) the height of Zhuonai Lake declined by 12.6 m after the outburst. In contrast, the heights of Kusai and Salt Lakes rose by 6.0 m (the mean of the C2 and J2 results) and 14.8 m (C2), respectively.

Using the two images in Fig. 8 and the lake level changes from C2 and J2, we computed the volume changes of Zhuonai, Kusai, and Salt Lakes as follows. First, we determine whether a pixel in the images is over lake water using the modified normalized difference water (MNDWI) index (Xu 2006):

$$MNDWI = \frac{G - MIR}{G + MIR} \qquad (4)$$

where G is the Green-band value and MIR is the middle infrared-band value. The pixels over lake water were then used to compute the lake areas from the two images (Table 2). Our result shows that, Zhuonai Lake lost an area of 111.9 km^2 due to the outburst, while Kusai and Salt Lakes gained areas of 42.8 and 81.4 km^2.

The changes in lake level (Fig. 9) and lake area (Table 2) were then used to determine the changes in volume
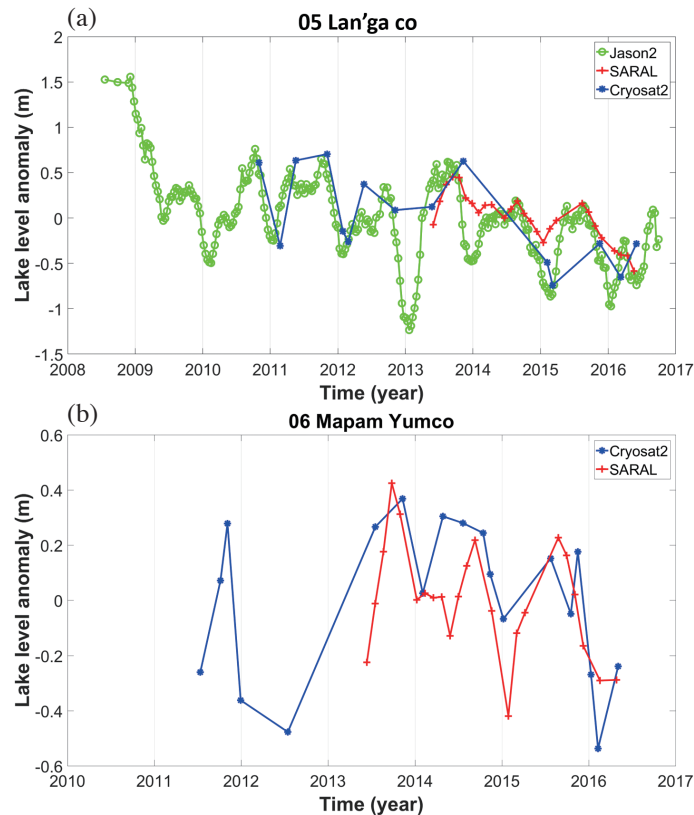
Fig. 6. Time series of lake level change over (a) La'nga Co and (b) Mapam Yumco.
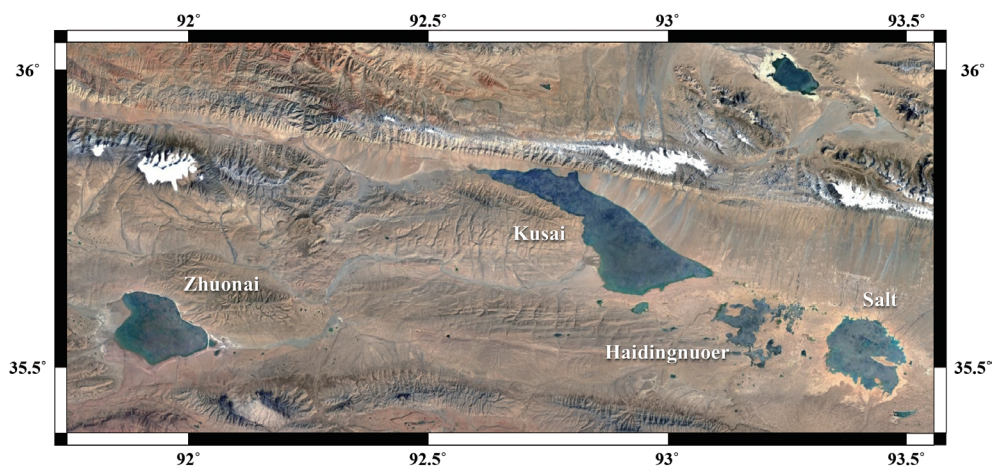
Fig. 7. Locations of Zhuonai Lake, Kusai Lake, Salt Lake, and Haidingnuoer Lake from the Google Earth. The frame of latitude and longitude is added by the authors of this paper.

Fig. 8. Landsat-7 images of Kusai and Salt Lakes on 23 November 2011 and 12 November 2012, showing different lake coverages before and after the 2011 lake outburst.
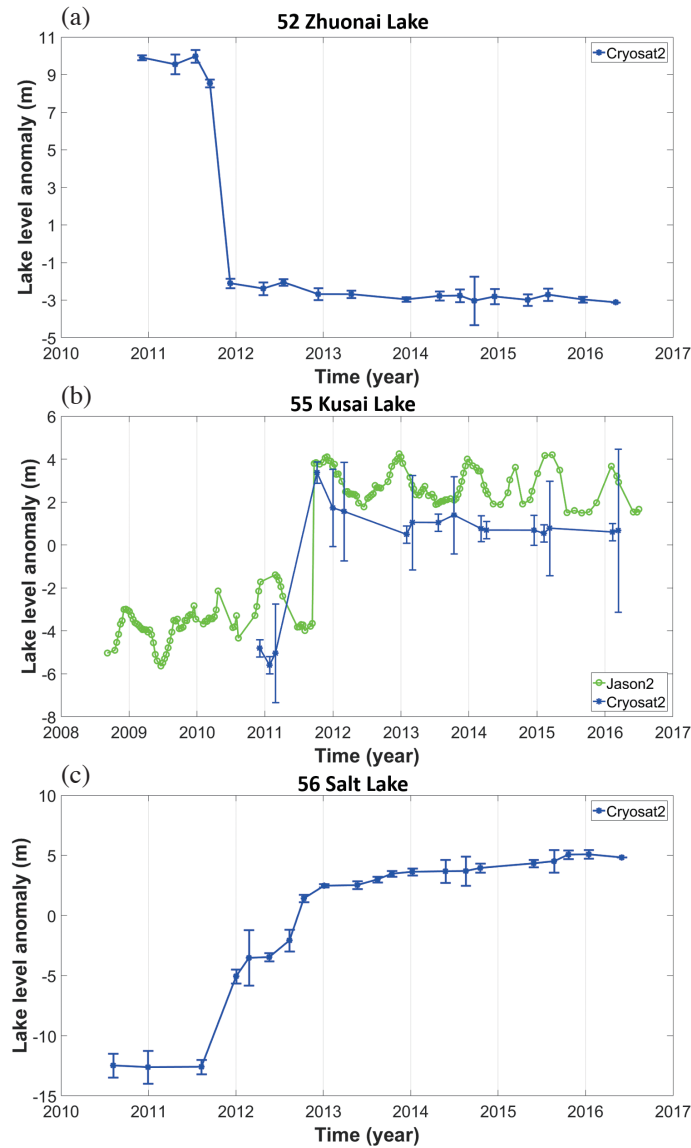
Fig. 9. (a) Drops of Zhuonai lake level in 2011 from Cryosat-2. (b) Rises of Kusai lake level from Cryosat-2 and Jason-2. (c) Rises of Salt lake level from Cryosat-2. The error bars correspond to the 68% confidence level (one sigma).

Table 2. Change of Zhuonai Lake area before and after the lake outburst (unit: km^2).

ID	Lake	Area (before outburst)	Area (after outburst)	Times of images (before/after)
52	Zhuonai Lake	253.8	152.2	2010/12/16 2012/11/03
55	Kusai Lake	275.3	327.2	2010/12/16 2012/11/03
56	Salt Lake	47.8	129	2010/11/23 2012/11/12

by two methods as follows (Taube 2000; Crétaux et al. 2016; Jiang et al. 2017):

$$\Delta V_1 = \frac{1}{3}(H_2 - H_1) \times (A_1 + A_2 + \sqrt{A_1 \times A_2}) \qquad (5)$$

$$\Delta V_2 = \frac{1}{2}(H_2 - H_1) \times (A_1 + A_2) \qquad (6)$$

where ΔV_1 and ΔV_2 volume change by the two methods, H_1 and H_2 are the lake levels before and after the lake outburst, and A_1 and A_2 are the areas before and after the outburst (Table 2). The first method [Eq. (6)] is more rigorous than the second method (Taube 2000).

Table 3 shows the volume changes using Eqs. (5) and (6). Both methods lead to the result that the sums of the three lake volume changes are not zero. This can be explained below. First, not only Kusai Lake and Salt Lake received runoff water from Zhuonai Lake, but also Haidingnuoer Lake, which is a small lake between Kusai Lake and Salt Lake. The original Salt Lake merged other minor lakes around it to quickly expand its area. As a result, the area and the positive lake volume may be overestimated. In addition, the times associated with the satellite images can influence the estimation of volume changes: their times may not exactly correspond to the times finalizing the net effect of water loss (Zhuonai Lake) and gain (Kusai Lake and Slat Lake). Lake shore gradients may also affect the extents of lake level changes, thereby affecting estimates of lake volume change. In general, under the same lake volume change, a gentle shore gradient will result in a less lake level change, compared to a steep shore gradient (Huang et al. 2012). In addition, the suddenly expanded areas of Kusai Lake and Salt Lake could be over shallow-water areas, which can lead to overestimated lake volume gains in the two lakes. The example around Kusai shows that multiple altimeters are useful in identifying the cause and effect of a lake outburst.

5. CONCLUSION

We used four altimeters: C2, SA, ICESat, and J2, to examine lake level changes in the TP. The C2's SARIn mode results in reliable lake level changes over a large number of lakes. Some of the rates of lake level change from C2 have been confirmed by the result from SA. A high spatial resolution of C2 can compensate for the deficiency in its temporal coverage, especially for the lakes with large areas that can be visited by a satellite like C2 during its 30-day sub-cycles. C2 has extended the lake level records from ICESat and repeat missions such as T/P and Jason-1 in some lakes, helping to understand the dominant contributing factors to the long-term lake level and climate changes in Tibet.

With its relatively small cross-track distance (7 km at the equator in one year), C2 can also detect water exchanges among lakes affected by extreme climatic events such as flooding. This capability was demonstrated over Zhuonai, Kusia, and Salt Lake using the volume losses and gains. Altimeter data from a repeat mission such as SA or J2 cannot achieve this because of its large cross-track spacing. Furthermore, the potential post-2016 lake level declines seen in many large lakes in the TP can be investigated using ongoing and future altimeter and GRACE data. It will be interesting to see whether such declining trends are transient or will continue into the next decade. This study shows the benefit of multiple altimeters for determining and cross-validating long term and episodic lake level changes in the TP.

REFERENCES

Biskop, S., F. Maussion, P. Krause, and M. Fink, 2016: Differences in the water-balance components of four lakes in the southern-central Tibetan Plateau. *Hydrol. Earth Syst. Sci.*, **20**, 209-225, doi: 10.5194/hess-20-209-2016. [Link]

Bouzinac, C., 2013: CryoSat Product Handbook, ESA, UCL, 150 pp. Available at https://earth.esa.int/documents/10174/125272/CryoSat_Product_Handbook.

Chao, N., Z. Wang, C. Hwang, T. Jin, and Y. S. Cheng,

Table 3. Volume changes of three lakes due to the 2011 lake outburst (unit: km^3).

ID	Lake	Volume change (Method 1)	Volume change (Method 2)
52	Zhuonai Lake	-2.5287	-2.5558
55	Kusai Lake	1.8233	1.8256
56	Salt Lake	1.2605	1.3092
	Sum	0.5551	0.5790

2017: Decline of Geladandong Glacier Elevation in Yangtze River's Source Region: Detection by ICESat and Assessment by Hydroclimatic Data. *Rem. Sens.*, **9**, 75, doi: 10.3390/rs9010075. [Link]

Crétaux, J. F., S. Calmant, V. Romanovski, A. Shabunin, F. Lyard, M. Bergé-Nguyen, A. Cazenave, F. Hernandez, and F. Perosanz, 2009: An absolute calibration site for radar altimeters in the continental domain: Lake Issykkul in Central Asia. *J. Geodesy*, **83**, 723-735, doi: 10.1007/s00190-008-0289-7. [Link]

Crétaux, J. F., R. Abarca-del-Río, M. Bergé-Nguyen, A. Arsen, V. Drolon, G. Clos, and P. Maisongrande, 2016: Lake volume monitoring from space. *Surv. Geophys.*, **37**, 269-305, doi: 10.1007/s10712-016-9362-6. [Link]

Fu, L. L. and B. J. Haines, 2013: The challenges in long-term altimetry calibration for addressing the problem of global sea level change. *Adv. Space Res.*, **51**, 1284-1300, doi: 10.1016/j.asr.2012.06.005. [Link]

Gao, L., J. Liao, and G. Shen, 2013: Monitoring lake-level changes in the Qinghai-Tibetan Plateau using radar altimeter data (2002-2012). *J. Appl. Remote Sens.*, **7**, 073470, doi: 10.1117/1.JRS.7.073470. [Link]

Huang, W., J. Liao, and G. Shen, 2012: Lake change in past 40 years in the southern Nagqu district of Tibet and analysis of its driving forces. *Remote Sensing for Land & Resources*, **24**, 122-128. (in Chinese)

Hwang, C., M. F. Peng, J. Ning, J. Luo, and C. H. Sui, 2005: Lake level variations in China from TOPEX/Poseidon altimetry: Data quality assessment and links to precipitation and ENSO. *Geophys. J. Int.*, **161**, 1-11, doi: 10.1111/j.1365-246X.2005.02518.x. [Link]

Hwang, C., Y. C. Kao, and N. Tangdamrongsub, 2011: A preliminary analysis of lake level and water storage changes over Lakes Baikal and Balkhash from satellite altimetry and gravimetry. *Terr. Atmos. Ocean. Sci.*, **22**, 97-108, doi: 10.3319/TAO.2010.05.19.01(TibXS). [Link]

Hwang, C., Y. S. Cheng, J. Han, R. Kao, C. Y. Huang, S. H. Wei, and H. Wang, 2016: Multi-decadal monitoring of lake level changes in the Qinghai-Tibet Plateau by the TOPEX/Poseidon-family altimeters: Climate implication. *Rem. Sens.*, **8**, 446, doi: 10.3390/rs8060446. [Link]

Immerzeel, W. W., L. P. H. van Beek, and M. F. P. Bierkens, 2010: Climate change will affect the Asian water towers. *Science*, **328**, 1382-1385, doi: 10.1126/science.1183188. [Link]

Jiang, L., K. Nielsen, O. B. Andersen, and P. Bauer-Gottwein, 2017: Monitoring recent lake level variations on the Tibetan Plateau using Cryosat-2 SARIn mode data. *J. Hydrol.*, **544**, 109-124, doi: 10.1016/j.jhydrol.2016.11.024. [Link]

Kang, S., Y. Xu, Q. You, W. A. Flügel, N. Pepin, and T. Yao, 2010: Review of climate and cryospheric change in the Tibetan Plateau. *Environ. Res. Lett.*, **5**, 015101, doi: 10.1088/1748-9326/5/1/015101. [Link]

Kleinherenbrink, M., R. C. Lindenbergh, and P. G. Ditmar, 2015: Monitoring of lake level changes on the Tibetan Plateau and Tian Shan by retracking Cryosat SARIn waveforms. *J. Hydrol.*, **521**, 119-131, doi: 10.1016/j.jhydrol.2014.11.063. [Link]

Kusche, J., R. Schmidt, S. Petrovic, and R. Rietbroek, 2009: Decorrelated GRACE time-variable gravity solutions by GFZ, and their validation using a hydrological model. *J. Geodesy*, **83**, 903-913, doi: 10.1007/s00190-009-0308-3. [Link]

Levine, A. F. Z. and M. J. McPhaden, 2016: How the July 2014 easterly wind burst gave the 2015-2016 El Niño a head start. *Geophys. Res. Lett.*, **43**, 6503-6510, doi: 10.1002/2016GL069204. [Link]

Liao, J., G. Shen, and Y. Li, 2013: Lake variations in response to climate change in the Tibetan Plateau in the past 40 years. *Int. J. Digital Earth*, **6**, 534-549, doi: 10.1080/17538947.2012.656290. [Link]

Liu, B. K., L. Lin, Y. Du, T. Liang, S. Duan, F. Hou and J. Ren, 2016: Causes of the outburst of Zonag Lake in Hoh Xil, Tibetan Plateau, and its impact on surrounding environment. *J. Glaciol. Geocryology*, **38**, 305-311. (in Chinese)

Liu, Z., 2012: Dynamics of interdecadal Climate Variability: A Historical Perspective. *J. Climate*, **25**, 1963-1995, doi: 10.1175/2011JCLI3980.1. [Link]

Navarra, A., 1999: Beyond El Niño: Decadal and Interdecadal Climate Variability, Springer-Verlag Berlin Heidelberg, Berlin, 375 pp, doi: 10.1007/978-3-642-58369-8. [Link]

Pavlis, N. K., S. A. Holmes, S. C. Kenyon, and J. K. Factor, 2012: The development and evaluation of the Earth Gravitational Model 2008 (EGM2008). *J. Geophys. Res.*, **117**, B04406, doi: 10.1029/2011JB008916. [Link]

Shao, Z., X. Meng, D. Zhu, D. Zheng, Z. Qiao, C. Yang, J. Han, J. Yu, Q. Meng, and R. Lü, 2008: Characteristics of the change of major lakes on the Qinghai-Tibet Plateau in the last 25 years. *Front. Earth Sci. China*, **2**, 364-377, doi: 10.1007/s11707-008-0038-5. [Link]

Song, C., Q. Ye, and X. Cheng, 2015: Shifts in water-level variation of Namco in the central Tibetan Plateau from ICESat and CryoSat-2 altimetry and station observations. *Sci. Bull.*, **60**, 1287-1297, doi: 10.1007/s11434-015-0826-8. [Link]

Tapley, B. D., S. Bettadpur, J. C. Ries, P. F. Thompson, and M. M. Watkins, 2004: GRACE measurements of mass variability in the Earth system. *Science*, **305**, 503-505, doi: 10.1126/science.1099192. [Link]

Tapley, B., F. Flechtner, M. Watkins, and S. Bettadpur, 2015: GRACE mission: Status and prospects. Presented at: Grace Science Team Meeting 2015, Austin, Texas.

Taube, C. M., 2000: Three methods for computing the volume of a lake. In: Schneider, J. C. (Ed.), Manual of Fisheries Survey Methods II: With Periodic Updates, Lansing, State of Michigan, United States of America: Michigan Department of Natural Resources.

Tseng, K. H., C. P. Chang, C. Shum, C. Y. Kuo, K. T. Liu, K. Shang, Y. Jia, and J. Sun, 2016: Quantifying freshwater mass balance in the central Tibetan plateau by integrating satellite remote sensing, altimetry, and gravimetry. *Rem. Sens.*, **8**, 441, doi: 10.3390/rs8060441. [Link]

Xu, H., 2006: Modification of normalised difference water index (NDWI) to enhance open water features in remotely sensed imagery. *Int. J. Remote Sens.*, **27**, 3025-3033, doi: 10.1080/01431160600589179. [Link]

Yang, K., H. Lu, S. Yue, G. Zhang, Y. Lei, Z. La, and W. Wang, 2018: Quantifying recent precipitation change and predicting lake expansion in the Inner Tibetan Plateau. *Clim. Change*, **147**, 149-163, doi: 10.1007/s10584-017-2127-5. [Link]

Yang, Y., C. Hwang, H. J. Hsu, E. Dongchen, and H. Wang, 2012: A subwaveform threshold retracker for ERS-1 altimetry: A case study in the Antarctic Ocean. *Comput. Geosci.*, **41**, 88-98, doi: 10.1016/j.cageo.2011.08.017. [Link]

Yao, X., S. Liu, L. Li, M. Sun, J. Luo, and Y. Feng, 2013: Spatial-temporal variations of lake area in Hoh Xil region in the past 40 years. *Acta Geogr. Sin.*, **68**, 886-896. (in Chinese)

Zhai, P., R. Yu, Y. Guo, Q. Li, X. Ren, Y. Wang, W. Xu, Y. Liu, and Y. Ding, 2016: The strong El Niño of 2015/16 and its dominant impacts on global and China's climate. *J. Meteorol. Res.*, **30**, 283-297, doi: 10.1007/s13351-016-6101-3. [Link]

Zhang, G., H. Xie, S. Kang, D. Yi, and S. F. Ackley, 2011: Monitoring lake level changes on the Tibetan Plateau using ICESat altimetry data (2003-2009). *Remote Sens. Environ.*, **115**, 1733-1742, doi: 10.1016/j.rse.2011.03.005. [Link]

Zhang, G., T. Yao, H. Xie, S. Kang, and Y. Lei, 2013: Increased mass over the Tibetan Plateau: From lakes or glaciers? *Geophys. Res. Lett.*, **40**, 2125-2130, doi: 10.1002/grl.50462. [Link]

Zhang, G., T. Yao, H. Xie, K. Zhang, and F. Zhu, 2014: Lakes' state and abundance across the Tibetan Plateau. *Chin. Sci. Bull.*, **59**, 3010-3021, doi: 10.1007/s11434-014-0258-x. [Link]

Zhang, G., T. Yao, S. Piao, T. Bolch, H. Xie, D. Chen, Y. Gao, C. M. O'Reilly, C. K. Shum, K. Yang, S. Yi, Y. Lei, W. Wang, Y. He, K. Shang, X. Yang, and H. Zhang, 2017a: Extensive and drastically different alpine lake changes on Asia's high plateaus during the past four decades. *Geophys. Res. Lett.*, **44**, 252-260, doi: 10.1002/2016GL072033. [Link]

Zhang, G., T. Yao, C. K. Shum, S. Yi, K. Yang, H. Xie, W. Feng, T. Bolch, L. Wang, A. Behrangi, H. Zhang, W. Wang, Y. Xiang, and J. Yu, 2017b: Lake volume and groundwater storage variations in Tibetan Plateau's endorheic basin. *Geophys. Res. Lett.*, **44**, 5550-5560, doi: 10.1002/2017GL073773. [Link]

Zhang, X., Y. Wu, and X. Zhang, 2015: Zhari namco water level change detection using multi-satellite altimetric data during 1992-2012. *J. Nat. Resour.*, **30**, 1153-1162, doi: 10.11849/zrzyxb.2015.07.008. (in Chinese) [Link]

APPENDIX A: SELECTED INFORMATION ABOUT THE STUDIED LAKES

Table A1. The following table shows selected information about the lakes where trends of lake levels are derived from Cryosat-2 and SARAL/AltiKa. Lake names are given in Chinese, English, and Tibetan (except Aksayqin Lake).

ID	Lake	Latitude(°)	Longitude (°)	Area (km²)	Mean height (m)	Altimeter
1	阿克賽欽 / Aksayqin Lake	35.17	79.85	174.3	4850	C2[1]
2	松木希錯 / Songmuxi Co / གཙུམ་བཞི་མཚོ	34.59	80.23	27.2	5057	C2
3	結則茶卡 / Jieze Caka / སྐྱེས་རྗེ་ཚྭ་ཁ	33.95	80.90	107.6	4530	C2/SA[2]
4	郭扎錯 / Gozha Co / ཀོ་བཀྲ་མཚོ	35.02	81.06	252.6	5086	C2
5	拉昂錯 / La'nga Co / ལག་ངར་མཚོ	30.65	81.24	268.5	4570	C2/SA
6	瑪旁雍錯 / Mapam Yumco / མ་ཕམ་གཡུ་མཚོ	30.72	81.47	412	4590	C2/SA
7	邦達錯 / Bamgdog Co / པང་བཏགས་མཚོ	34.94	81.55	106.5	4909	C2/SA
8	魯瑪江東錯 / Lumachangdong Co / ལུ་མ་བྱང་སྟོང་མཚོ	34.04	81.62	351.6	4818	C2/SA
9	普爾錯 / Pur Co / ཕུར་མཚོ	34.88	81.96	40.12	5054	C2

Note: 1: Cryosat-2; 2: SARAL/AltiKa.

Table A1. (Continued)

ID	Lake	Latitude(°)	Longitude (°)	Area (km²)	Mean height (m)	Altimeter
10	黑石北湖 / Heishi North Lake / ནེ་ཧྲི་བའི་མཚོ	35.55	82.75	93	5055	C2/SA
11	昂拉仁錯 / Ngangla Ringco / ངང་ལྷ་རིང་མཚོ	31.54	82.99	512.7	4721	C2/SA
12	拜惹布錯 / Bairab Co / དཔལ་རབ་མཚོ	34.99	83.07	128.8	4966	C2
13	鹹水湖 / Salt Water Lake / བྲུལ་ཆུ་མཚོ	35.29	83.12	88.9	4894	C2
14	仁青休布錯 / Rinqin Xubco / རིན་ཆེན་ཤུབས་མཚོ	31.28	83.46	187.1	4765	C2
15	塔若錯 / Taro Co / ཐ་རོ་མཚོ	31.14	84.12	486.6	4572	C2/SA
16	拉果錯 / Lagkor Co / ལག་སྐོར་མཚོ	32.02	84.12	91.2	4472	C2
17	羊卓雍措 / Yamzhog Yumco / ཡར་འབྲོག་གཡུ་མཚོ	35.42	84.64	90	4783	C2
18	洞錯 / Dong Co / སྦོང་མཚོ	32.18	84.74	123.5	4399	C2/SA
19	達瓦錯 / Dawa Co / ཟླ་བ་མཚོ	31.24	84.96	114.4	4628	C2
20	佩枯錯 / Peiku Co / པད་ཁུད་མཚོ	28.83	85.6	284.4	4585	C2
21	扎日南木錯 / Zhari Nam Co / བཀྲ་རི་གནམ་མཚོ	30.93	85.6	996.9	4617	C2/SA
22	依布茶卡 / Yi'bug Caka / གཡི་སྦུག་ཚྭ་ཁ	32.86	86.66	88	4563	C2
23	湧波錯 / Yurbao Co / གཡུར་རྣ་མཚོ	35.74	86.72	58.2	4887	C2
24	瑪爾蓋茶卡 / Margai Caka / དམར་གད་ཚྭ་ཁ	35.12	86.77	79.6	4798	C2
25	昂孜錯 / Ngangzi Co / ངང་རྩེ་མཚོ	31.02	87.12	461.5	4690	C2/SA
26	達則錯 / Dagze Co / སྟག་རྩེ་མཚོ	31.89	87.54	244.7	4470	C2/SA
27	吳如錯 / Urru Co / ཨུར་རུ་མཚོ	31.71	88.01	342.7	4559	C2
28	仙鶴湖 / Xianhe Lake / གསན་ཧྲེའི་མཚོ	35.99	88.09	33.4	4846	C2
29	銀波湖 / Yinbo Lake / ཡིན་པོ་མཚོ	36.19	88.13	30.4	4882	C2
30	朋彥錯 / Pongyin Co / པོང་དཉི་མཚོ	32.89	88.19	48.8	4732	C2
31	雪梅湖 / Xuemei Lake / ཞོད་སྨད་མཚོ	36.27	88.25	33.5	4878	C2/SA
32	格仁錯 / Gyaring Co / སྐེ་རིང་མཚོ	31.04	88.45	475.9	4654	C2/SA
33	令戈錯 / Linggo co / སྒྲིང་གོ་མཚོ	33.85	88.59	89	5068	C2
34	多格錯仁 / Dogai Coring / རྡོ་སྐས་མཚོ་རིང	34.57	88.99	393.3	4823	C2/SA
35	色林錯 / Selin Co / སེར་སྒྲིང་མཚོ	31.81	89.01	2391	4544	C2/SA
36	多格錯仁強錯 / Dogaicoring Qangco / རྡོ་སྐས་མཚོ་རིང་བྱང་མཚོ	35.32	89.20	207.5	4792	C2/SA
37	鯨魚湖 / Jingyu Lake / ཆུ་སྲིན་མཚོ	36.35	89.38	320.33	4718	C2/SA
38	多爾索洞錯 / Dorsoidong Co / གདོར་ཟོལ་གདོང་མཚོ	33.38	89.86	400	4935	C2/SA
39	波濤湖 / Botao Lake / རྦ་རླབས་མཚོ	34.00	89.95	70.9	4994	C2
40	其香錯 / Kyebxang Co / ཁྱེ་བཟང་མཚོ	32.44	89.98	149	4620	C2
41	勞日特錯 / Laorite Co / ལོའི་རི་ཐེ་མཚོ	33.72	90.03	57.3	4955	C2
42	勒斜武擔湖 / Lexie Wudan Lake / ལེ་ཤེ་ཨོ་སྟན་མཚོ	35.74	90.18	231.2	4875	C2/SA

Table A1. (Continued)

ID	Lake	Latitude(°)	Longitude (°)	Area (km²)	Mean height (m)	Altimeter
43	赤布張錯 / Chibuzhang Co / མེ་རིག་རྐྱང་གྲམ་མཚོ	33.46	90.21	476.8	4941	C2/SA
44	西金烏蘭湖 / Xijir Ulan Lake / བི་ཅིན་ཡུ་ལན་མཚོ	35.20	90.34	530	4780	C2
45	烏蘭烏拉湖 / Wulanwula Lake / ཡུ་ལན་ཡུ་ལ་མཚོ	34.75	90.39	610	4777	C2/SA
46	普莫雍錯 / Puma Yumco / ཕུ་མ་གཡུ་མཚོ	28.56	90.40	295	5019	C2/SA
47	納木錯 / Nam Co / གནམ་མཚོ	30.71	90.53	1920	4729	C2/SA
48	明鏡湖 / Mingjing Lake / མེ་ལོང་མཚོ	35.06	90.54	121.2	4802	C2/SA
49	太陽湖 / Taiyang Lake / ཉི་མ་མཚོ	35.92	90.63	99.8	4886	C2
50	茲格塘錯 / Zige Tangco / ཅི་གེ་དར་མཚོ	32.06	90.84	191.4	4573	C2
51	可可西里湖 / Hoh Xil Lake / ཨ་ཆེན་གངས་རྒྱབ་མཚོ	35.58	91.15	347.3	4892	C2
52	卓乃湖 / Zhuonai Lake / གཙོད་གནས་མཚོ	35.54	91.93	51	4758	C2
53	錯仁德加 / Cuorendejia / མཚོ་རི་བདེ་རྒྱལ	35.21	92.20	192.3	4693	C2/SA
54	特拉什湖 / Telashi Lake / ཐེ་ལྦ་ཤྲེད་མཚོ	34.80	92.21	54.1	4810	C2
55	庫賽湖 / Kusai Lake / ཁུ་སེ་མཚོ	35.69	92.92	336.17	4480	C2/SA
56	鹽湖 / Salt Lake / ཚྭ་ཁ	35.52	93.40	124.9	4450	C2
57	扎陵湖 / Gyaring Lake / མཚོ་སྐྱ་རིང	34.93	97.27	526	4295	C2/SA
58	鄂陵湖 / Eling Lake / མཚོ་སྣོ་རིང	34.88	97.68	610	4272	C2/SA
59	冬給措納湖 / Donggei Cuona Lake / གདོང་གཀའི་མཚོ་ནག	35.26	98.60	226.5	4270	C2
60	阿拉克湖 / ALake Lake / ཨ་ལ་ཁེ་མཚོ	35.56	97.13	47	4110	SA
61	青海湖 / Qinghai Lake / མཚོ་སྔོན་པོ	36.76	100.35	4186	3198	SA